Accurate position estimation methods based on electrical impedance tomography measurements

Samuel Vergara[1*], Daniel Sbarbaro[1], T. A. Johansen[2]

[1] Electrical Engineering Department, Faculty of Engineering, University of Concepción, Chile

[2] Center for Autonomous Marine Operations and Systems. Department of Engineering Cybernetics, Norwegian University of Science and Technology NTNU, O.S. Bragstads plass 2D, N-7491 Trondheim, Norway.

*E-mail: svergara@udec.cl

Abstract

Electrical impedance tomography (EIT) is a technology that estimates the electrical properties of a body or a cross section. Their main advantages are its non-invasiveness, low cost and free of radiation operation. The estimation of the conductivity field leads to low resolution images compared with other technologies and high computational cost. However, in many applications the target information lies in a low intrinsic dimensionality of the conductivity field. The estimation of this low dimensional information is addressed in this work. It proposes optimization based and data driven approaches for estimating this low dimensional information. The accuracy of the results obtained with these approaches depends on modelling and experimental conditions. Optimization approaches are sensitive to model discretization, type of cost function and searching algorithms. Data driven methods are sensitive to the assumed model structure and the data set used for parameter estimation. The system configuration and experimental conditions such as number of electrodes and signal noise ratio have also an impact on the results. In order to illustrate the effects of all these factors, the position estimation of a circular anomaly is addressed. Optimization methods based on weighted error cost functions and derivate free optimization algorithms provided the best results. Data driven approaches based on linear models provided, in this case, good estimates, but the use of nonlinear models enhanced the estimation accuracy. The results obtained by optimization based the algorithms were less sensitive to experimental conditions, such as number of electrodes and signal noise, than Data driven approaches. Position mean squared errors for simulation and experimental conditions were more than twice for the optimization based approaches compared with the data driven. Experimental position estimation mean squared error of data driven models using a 16 electrodes setup was less than 0.05% of tomograph radius value. These results demonstrate that the proposed approaches can estimate objects position accurately based on EIT measurements, if enough process information is available for training or modelling. Since they do not require complex calculations it is possible to use them in real-time applications without requiring high performance computers.

Keywords: Electrical Impedance Tomography, Optimization, anomaly location.

INTRODUCTION

Conductivity distribution imaging obtained by Electrical Impedance Tomography (EIT) sensors provides nonintrusive measurements for a wide range of industrial applications [1–4] and medical applications [5–7]. Position estimation is a relevant problem for both applications. Some examples are the position detection of internal bleeding, lung anomalies[8,9] and gas bubbles location in multiphase flows or fluidized beds [10–12].

EIT is a low cost, fast, non-invasive and radiation-free technology. It can estimate the conductivity (Electrical Resistance Tomography; ERT) and/or capacitance (Electrical Capacitance Tomography; ECT) distribution of a body or a cross-sectional area. This estimation requires solving a nonlinear ill-posed inverse problem. Typical approaches consider iterative image reconstruction algorithms such Gauss-Newton or Levenberg-Marquardt with some regularization term [13–18]. Some of these methods use prior knowledge of the domain or process to obtain the solution. However, to obtain high quality images it is required to use numerical techniques such finite elements method (FEM) with fine meshes. This implies a high computational cost.

In [19] is proposed an evaluation methodology for EIT systems. Image reconstruction was carried out by a parameterized one step Gauss-Newton algorithm. The methodology considers the estimation of different parameters of test objects images in a systematic way. One of the parameters was the object position estimation (PE). The object position was referenced to the center of gravity of the reconstructed object. Normalized errors by diameter position obtained an approximated maximum normalized error of 0.3. This is a 30% of system radius value. Also in [19] was stated the importance of having accuracy in PE, because its errors may lead to unreliable interpretation of the images.

In [20] study the performance of Sheffield, GREIT and Gauss-Newton algorithms for the PE and other parameters were analysed. PE results showed small error close of the center and increased errors close of the boundary, where the system has increased sensitivity. Location and size of anomalies were estimated in [9] using a simple weighted combinations of injection current and boundary voltage, but the method requires an injection current pattern that generates an uniform electric field. It may not be possible to find such a pattern for an arbitrary conductivity distribution. Some authors have proposed to determine this information using parametric methods [20]. These methods assume that the anomaly can be parameterized in terms of few parameters. These parameters were obtained by solving the forward problem using the boundary element method and optimization algorithms. The shape and position of anomalies was estimated in [21] and [22]. In both studies an optimization problem is stated and the object contour is estimated using a truncated Fourier series model. The first approach used a particle filter while last one used Hooke and Jeeves pattern search method to solve the problem. Both solutions showed high accuracy for a single object, however computational requirements are high. The different factors affecting the accuracy of the estimates was not analysed in these works.

There are applications, however, that do not require to reconstruct accurately the conductivity field, because the process underlying information lies in a set of low dimensional features. For instance, in industrial processes, monitoring of heterogeneous phases is important to the safety and operation of the engineering structures. Particularly, the visualization of voids and gas bubbles is advantageous; then information required is only its size, shape and position. Exploiting this process knowledge could be a way to obtain high accuracy, low computational complexity and robust methods who are needed for industrial applications [23]. In [24] and [25] the conductivity distribution was described as nonlinear function considering a set of parameters related to object and medium properties. This function implicitly regularizes the problem, so no additional regularization terms is needed.

The low dimensionality of position estimation problem was addressed in [26] by using methods based in optimization and data driven models. In the present work, the results of [26] are expanded by analysing the influence of different factors such as: model discretization, type of cost functions for position estimation and optimization algorithms. In addition, the combination of data driven models to enhance the accuracy of its predictions is also explored.

This paper is organized as follows: Section 1 describes the EIT model and defines the problem. Section 2 describes the general framework for solving the problem of low dimensional feature estimation. Section 3 describes the position estimation problem and solution methods. Section 4 outlines the simulation parameters and analyses the simulation results. Section 5 describes the experimental setting and experimental results. Finally, in sections 5 and 6 the discussion and conclusion of this work are presented.

1 EIT Model and Problem Definition

An EIT sensor system has a set of L electrodes placed on the boundary of a region of interest. A current is injected in a predefined pattern using two electrodes each time and the induced potentials are measured between adjacent remaining ones. The set of electrodes pairs used to voltage measuring and current injection are called measurement and injection pattern[6]. In this study the neighbourhood measurement/injection pattern was used. The number of measurements N_m will depend on the number of electrodes and injection/measurement strategy. The EIT sensor model considers an object $\Omega \subset R^3$ with a given conductivity distribution $\sigma(z,t), z \in \Omega$. The electrical currents i_j are injected into the object Ω through electrodes having a surface e_j located on the boundary $\partial\Omega$. Then, the induced electrical potential u and the voltages v_j can be uniquely determined by solving the equation (1) subject to conditions (2)-(4) comprising partial differential equations, which defines the complete electrode model:

$$\nabla\,(\sigma\,\nabla\,u) = 0 \;\; in\;\Omega \tag{1}$$

$$u + \alpha_j\,\sigma\,\frac{\partial u}{\partial r} = v_j \quad on\; e_j, j = 1,2,\ldots,\mathrm{L} \tag{2}$$

$$\int_{e_j} \sigma\,\frac{\partial u}{\partial r}\,ds = i_j \;\; j = 1,2,\ldots,L \tag{3}$$

$$\sigma \frac{\partial u}{\partial r} = 0 \quad on\ \partial\Omega \setminus \bigcup_{j=1}^{L} e_j \tag{4}$$

Let $P \subset \Omega \subset R^3$ be an object with boundary ∂P in Ω with conductivity σ_p placed in a medium of homogeneous conductivity σ_0. The conductivity σ_p is a function of a vector of low dimensional features represented by $X \in R^n$, where n is the number of features to be estimated.

The problem addressed in this work is to estimate the low dimensional features vector X based on the measured boundary voltages v_j.

2 LOW DIMENSIONAL FEATURES ESTIMATION

2.1 Optimization Approach

This approach requires enough knowledge of the process to formulate a forward problem $\hat{U}(\hat{\sigma}(\hat{X}))$ and solve the complete electrode model. As example the following information could be known: the conductivities σ_0 and $\sigma_p(X)$, dimensions and boundaries of Ω and P. The model inputs are the estimated conductivity distribution $\hat{\sigma}$ that varies according the estimated $\hat{X}$; $i.e. \hat{U}\left(\hat{\sigma}\left(\hat{X}\right)\right) = \hat{U}(\hat{X})$.

A cost function $F(\hat{X})$ considering the residual error between the measured and simulated voltages can be obtained by using the forward model. Constraints could also be considered.

We compared the use of two cost functions for the optimization problem: Non-linear least squares (NLS) (5)

$$\min_{\hat{X}} \left\| \hat{U}(\hat{X}) - U(X) \right\|_2^2 \tag{5}$$

and a weighted NLS we refer as Non-linear relative error least squares (NRLS) (6) to emphasize the difference to the classical weighted least squares based on covariance matrix.

$$\min_{\hat{X}} \left\| \Lambda\big(U(X)\big)^{-1} \left(\hat{U}(\hat{X}) - U(X) \right) \right\|_2^2 \tag{6}$$

Here $U(X)$ represents the measured voltages and $\Lambda\big(U(X)\big)$ is a diagonal matrix having in its diagonal the elements of vector $U(X)$. The forward problem of computing $\hat{U}(\hat{X})$ is solved by using the finite elements method (FEM) [27]. By optimizing over $\hat{X}$ instead of $\hat{\sigma}$, less demanding image quality requirements are imposed, allowing coarse mesh elements and lowering associated computational costs.

2.2 Data driven approach

The relationship between the measured voltages and the object features is described by parametric models. Data driven approaches give a direct mapping from measured voltages and object feature avoiding the problem introduced by using approximated solutions provided by numerical models. The validity of these models depends on the type of parametrization and the data set used for estimating the parameters. Linear and nonlinear parameterizations can be used to represent the relationship, as described below.

2.2.1 *Linear parameterization*

Let $U(\sigma)$ be the vector containing the voltage measurements corresponding to all current patterns. A linearized mapping of $U = U(X) = U(\sigma(X))$ in a condition with features vector $X_0 \in R^n$ is:

$$U(X) - U(X_0) = \frac{\partial U(\sigma(X_0))}{\partial X}(X - X_0) \tag{7}$$

Solving for X a direct mapping from measured voltages is obtained using the pseudo-inverse:

$$X = \left[\frac{\partial \bar{U}(\hat{\sigma}(X_0))}{\partial X}\right]^{\dagger} U(X) - \left[\left[\frac{\partial \bar{U}(\hat{\sigma}(X_0))}{\partial X}\right]^{\dagger} U(X_0) - X_0\right] \tag{8}$$

Equation (9) can be written as

$$X = \Theta U_e \tag{9}$$

where $\Theta = \left[\left[\frac{\partial \bar{U}(\hat{\sigma}(X_0))}{\partial X}\right]^{\dagger} \quad \left[\left[\frac{\partial \bar{U}(\hat{\sigma}(X_0))}{\partial X}\right]^{\dagger} U(X_0) - X_0\right]\right]$ and $U_e(X) = [U(x)^T \quad -1]^T$.

In general, analytical expressions for the partial derivatives are not available, but the parameters of the model (9) can also be obtained by solving a least squares problem:

$$\min_{\Theta} \|\Theta U_e - U(X)\|_2^2 \tag{10}$$

The main advantages of this approach are its simplicity and calculation speed. However, its application may be limited since it requires a large training data set for having a well-conditioned optimization problem and linearization may be valid only in a small neighborhood of X_0.

2.2.2 *Non-linear parameterization*

In general non-linear representations will provide models with a wider validity range

$$X = N(\Theta, U_e)$$

where $N(\Theta, U_e)$ is a nonlinear function defined in terms of a set of parameter vector Θ. In this context, the estimation problem can be split into two sub-problems: find suitable model structure and estimate its parameters from a finite set of data. This problem is ill-posed, but as pointed out in ([28]) a minimum of prior knowledge will be enough, in general, to provide the necessary constraints for obtaining reasonable solutions. Analytical model describing the measured voltages and features are not available, but some physical insight can be used to suggest nonlinear combinations of measured data signals. A basic general rule in estimation one should utilize prior knowledge and physical insight about the system when selecting the model structure [29].

If no physical insight is available or used, the use of flexible parametrization such as Support Vector Machines or Neural Networks can provide reasonable results. Statistical methods [28,30,31] provide effective frameworks for combining prior knowledge and empirical data.

The model fidelity of data driven models can only be ensured if the training set is representative of the conditions under which the model will be used.

2.3 Estimation Errors Sources

There are many factors affecting the accuracy of these methods. They can be classified according to their origin; i.e. experimental or modelling.

2.3.1 Experimental sources

Multiple aspects of experimental conditions can affect the feature vector estimation. The most obvious is measurement error because it will generate differences with simulated situations. Another factor is the EIT equipment features as instrumentation accuracy, number of electrodes and injection measurement pattern. The first one sets the sensitivity required to differentiate the conductivity between the medium and target. The others features define the amount of measurements available, sensitivity distribution and distinguishability [32–34]. Also sensitivity improvement is achieved with a larger number of electrodes and a reduction in the ill-posed condition of the Hessian approximation that consequently improves the reconstruction [35]. However according to [36] a larger number of electrodes do not ensure a better reconstruction of lung contours.

2.3.2 Modelling sources

There are several sources for modelling errors. The number of elements and nodes, elements basis functions order of FEM [27,35,37], mismatch in domain boundary, time varying boundary [38–41] and model discretization[42–44]. Simplifications assumptions such as that current travels only in a two-dimensional plane and that conductivity in domain do not changes severely between several injections (static EIT) are also source of errors. Changes in temperature and pH are usually neglected, but in some applications they should also be taken into account.

Modelling errors associated to contact impedances are also important, [45] investigates the effect of errors in electrode contact impedance, electrode area, and boundary shape under the electrode in two-dimensional difference EIT reconstructions.

Several techniques have been proposed to deal with some of these factors as been proposed in [35, 41, 42]. A model calibration procedure was used in this work to reduce these effects [47]. Modelling errors affects estimation methods based on optimization but do not affect data driven approaches. The effect of modelling discretization is simulated and discussed.

3 CASE STUDY: POSITION ESTIMATION

The position estimation of an object of known shape and conductivity is presented in this section to illustrate the different factors affecting the accuracy of the estimations. A 2D problem of imaging the cross section of a circular section anomaly in a cylindrical vessel was carried out. The anomaly's conductivity was 10 times lower than the medium. The EIT system had a set of 16 electrodes at the boundary of the vessel. A neighbourhood injection and measurement pattern was used to obtain a total of $L(L-3)$ =208 voltage measurements per sampling instant.

3.1 Optimization Approach

In this case, the model inputs are the estimated conductivity distribution $\hat{\sigma}$ that varies according the estimated object position $\hat{X}$, consequently $\hat{U}\left(\hat{\sigma}\left(\hat{X}\right)\right) = \hat{U}(\hat{X})$. The cost functions (5) and (6) are

considered. As pointed out in section 2.3.2 the cost surfaces are affected by model discretization. This generates a rough surface that could generate local minimum points. An analysis about how optimization methods are affected by discretization will be carried out in section 4. Gradient based Non-Linear least squares optimization (GBNLLSO) and derivative free (DFO) optimization techniques are considered. The solvers were selected from the OPTI toolbox [48] and MATLAB 2013a and are described in Table I.

Table I. OPTIMIZATION SOLVERS DESCRIPTIONS

Search Method	*Optimization Type*	*Description*
LMDER	GBNLLSO	Levenberg-Marquardt routine for solving NLS problems. It obtains the gradient by finite differences.
NLOPT	GBNLLSO	Implementation of the Augmented Lagrangian algorithm described in [49,50]. It can handle non-linear equality/inequality constraints.
OPTI_FMINUNC	GBNLLSO	Solves NLS problems using a Quasi-Newton method with a cubic line search procedure. It uses BFGS to update the Hessian approximation[51].
PSWARM	DFO - Genetic Algorithm	This search method solves non-differentiable, linearly constrained, nonlinear programs using a dual pattern and particle swarm algorithm[52].
PATTERNSEARCH	DFO	Implementation of a generalized pattern search (GPS) algorithm. This numerical method do not requires the problem gradient[53].
NOMAD	DFO	An extension of the GPS algorithm. Nonlinear Optimization with the mesh adaptive direct search (MADS) algorithm. It can solve non-differentiable and global nonlinear problems.
FMINSEARCH	DFO	MTALAB's multidimensional unconstrained nonlinear minimization with the Nelder-Mead algorithm.

3.2 Data driven approaches

Two simple models based on Cartesian and Polar coordinates are considered in this section. The main advantage of these approaches is their simplicity and calculation speed. However, their application is limited, since access to large training data is required and linearization may be valid only in a small neighborhood of X_0.

3.2.1 Cartesian Coordinates Model

Let $U(\sigma)$ be the vector containing the voltage measurements corresponding to all current patterns. Equation (9) can be used directly to obtain the position in features vector $\hat{X}$

3.2.2 Polar Coordinates Model

The polar model is a nonlinear model and get the position of the object since the estimation in terms of an angle θ and a magnitude r. Due the discontinuity of θ is not possible get a linear model. Thus θ is estimated using:

$$\hat{\theta} = \tan^{-1}\left(\frac{\hat{X}_2}{\hat{X}_1}\right) \tag{11}$$

where $\hat{X} = [\hat{X}_1\ \hat{X}_2]^T$ is the position estimated by linear model in Cartesian coordinates (9). The position magnitude is modelled as a linear combination of the measured voltages as:

$$\hat{r} = \Theta_r\, U_e \tag{12}$$

With $\Theta_r \in R^{1\times(N_m+1)}$ is a vector of parameters. Then

$$\hat{X}_{\hat{r},\hat{\theta}} = \begin{bmatrix} \hat{r}\cos(\hat{\theta}) \\ \hat{r}\sin(\hat{\theta}) \end{bmatrix} \quad (13)$$

In present work, matrices Θ_r and Θ were obtained using random training data points and least squares identification by solving (10) .

3.3 Evaluation criteria

Evaluation of simulation and experimental results are quantified by the Mean Squared Error (MSE) according equation (14) where N_m is the number of samples.

$$MSE = \frac{1}{N_m}\sum_{i}^{N_m}\left(X_i - \hat{X}_i\right)^T\left(X_i - \hat{X}_i\right) \quad (14)$$

The simulations were carried out under different SNR values calculated according (15), where A_s is the signal amplitude and A_n is the maximum noise amplitude. A maximum SNR was set and a random value was applied to each measurement. It should be noted that the same contaminated data was used for all the search methods in the optimization approach simulations.

$$SNR = 20\log\left(\frac{A_s}{A_n}\right) \quad (15)$$

The simulations and experiments results shows all the distances normalized with the tomograph radius.

4 SIMULATIONS RESULTS

The simulations were carried using the EIDORS toolbox[54]. In order avoid an inverse crime, the FEM model for simulating the measured voltages considered 6400 elements, while the mesh used to the forward model in optimization approach had 576 elements. Medium and target conductivity were $2.66 \cdot 10^{-4}[S/m]$ and $1 \cdot 10^{-6}[S/m]$ respectively.

Position estimation by optimization approach requires a correct and accurate modelling of the voltage distributions. To reduce differences between models output, a model calibration process was achieved. The process used was developed in [47] and it consist in three steps. The first step is obtaining the scaling factors. These are calculated as the ratio of the homogeneous forward solution to the corresponding experimental measurement. The next step is the calculation of the global property values. These are the estimations of the electrical properties that minimize the output model error compared with a known condition, in this case, the homogenous medium situation. We obtained them by solving a NLS optimization problem (16). Finally an offset removal stage was done. Hence calibrated voltages are obtained as the scaled simulation minus two offset terms. The first term is the difference between a homogenous measurement and its scaled simulation with global property values. The second is the difference between an anomaly experiment measurement

and its scaled simulation. We neglected this last term because the offset induced by the object will vary according to its position in the tomograph.

$$\min_{\hat{\sigma}} \left\| \hat{U}(\hat{\sigma}) - U(\sigma_0) \right\|_2^2 \tag{16}$$

The simulations were carried in Windows 7 64 bits environment by using MATLAB 2013a software and EIDORS and OPTI toolboxes. They were carried out on a personal computer with an Intel i7 processor and 8 GB RAM.

4.1.1 Optimization approach

Modelling Error Sources

The FEM Model accuracy depends of multiple factors such as: the number of elements, their size and distribution. Coarse meshes fail to represent accurately the objects due that elements do not match with object shape (Figure 1). Table II summarizes some calculated features: coordinates of the target centroid and its area. All the elements with conductivity higher than the background were considered to get the target area. It can be seen that a larger number of elements does not imply a better object representation. Obviously decreasing the size of the elements, will diminish this effect, however it implies an increment of computational cost. Furthermore it could be easy to adjust the shape of elements to objects shape for forwards problems, but in the inverse problem it is not so straight forward and additional components should be included in the reconstruction process to avoid image artefacts appearing in the reconstructed images[44].

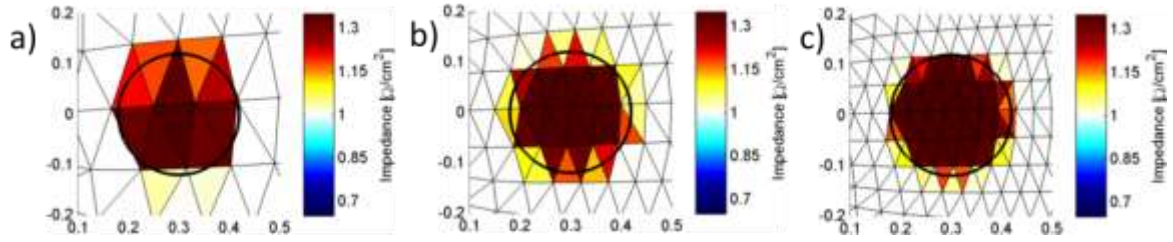

Figure 1. Target shape deformation by mesh elements approximation. Bold lines show the real object boundary. Thin lines shows elements contour. a) 576 elements mesh. b) 1600 elements mesh. c) 3126 elements mesh.

Table II. FEATURES CHANGES BY DISCRETIZATION

	Real value	576 elements mesh	1600 elements mesh	6400 elements mesh
x coordinate	3,00E-01	3,01E-01	3,05E-01	3,00E-01
y coordinate	0	-1,64E-02	4,82E-03	-8,00E-05
Object area	4,52E-02	7,06E-02	7,46E-02	6,41E-02

The cost function surfaces obtained by meshes of 576, 1600 and 3136 elements are depicted in Figure 2 for a reference position at [0, 0.5]. Figure 3 shows the existence of local minimums in a neighborhood of the real object position. These minimums exist due the domain discretization. This effect seems less severe in finer mesh models; however even a fine mesh did not ensure a

continuous surface. The error between the minimum location and the real object position is decreased as a function of the number of mesh elements (see Table II). Smaller errors were obtained by using the weighted cost function NRLS than NLS.

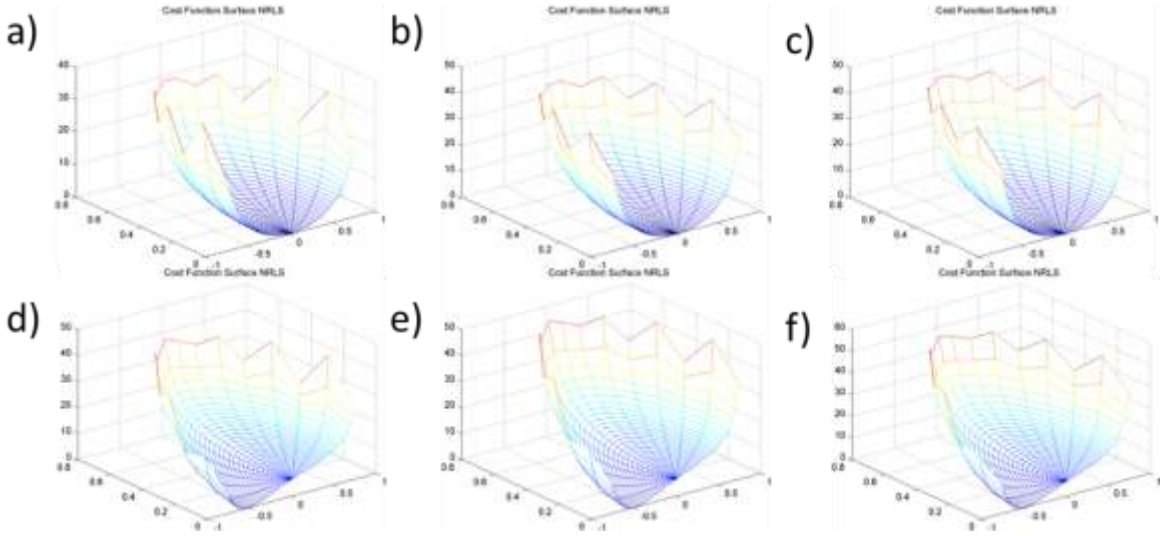

Figure 2. Cost surfaces of NRS and NRLS problems for an object reference position at [0,0.5]. Top row NLS. Bottom row NRLS a,d)Forward mesh of 576 elements b,e) Forward mesh of 1600 elements c, f) Forward mesh of 3136 elements.

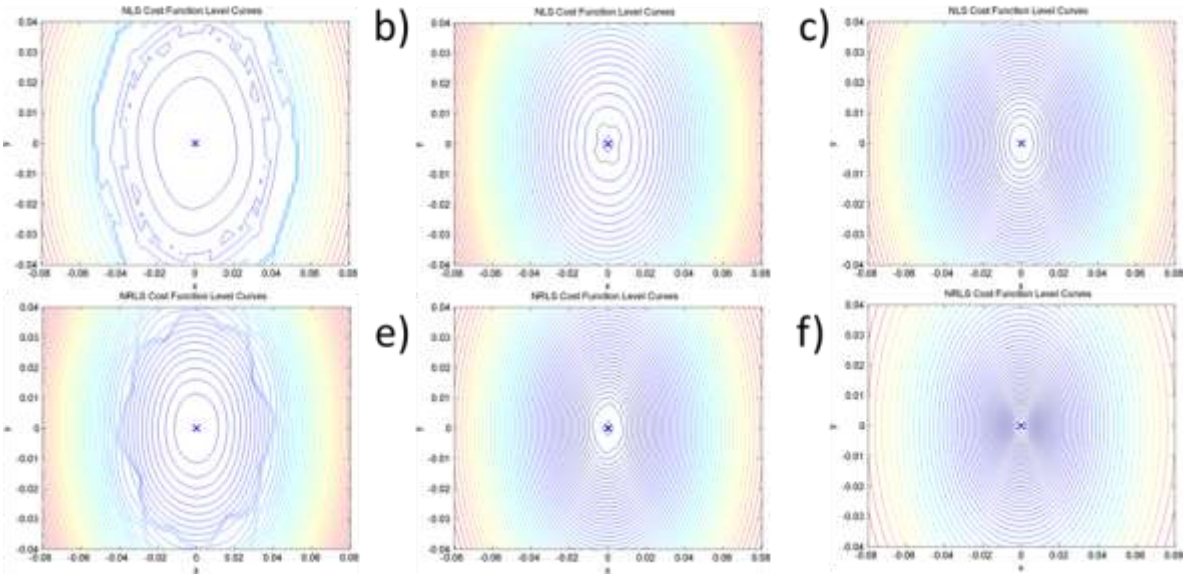

Figure 3. Level cost curves of NLS and NRLS problems for an object reference position at [0,0](center marked with a blue x). Top row NLS. Bottom row NRLS a,d)Forward mesh of 576 elements b,e) Forward mesh of 1600 elements c, f) Forward mesh of 3136 elements.

Experimental Conditions and Optimal Search Methods

To evaluate the effect of the number of electrodes in the position estimation of an object at the origin, the optimization problem using the same mesh but with 8, 16 and 32 electrodes was solved (Figure 4). A mesh of 6400 elements was used as reference and 4096 elements mesh was used for

minimization. The results showed that incrementing the number of electrodes has a negative effect in the optimization surface. The gradient in the neighborhood of the minimum is smaller so gradients search methods will advance slowly or get stuck.

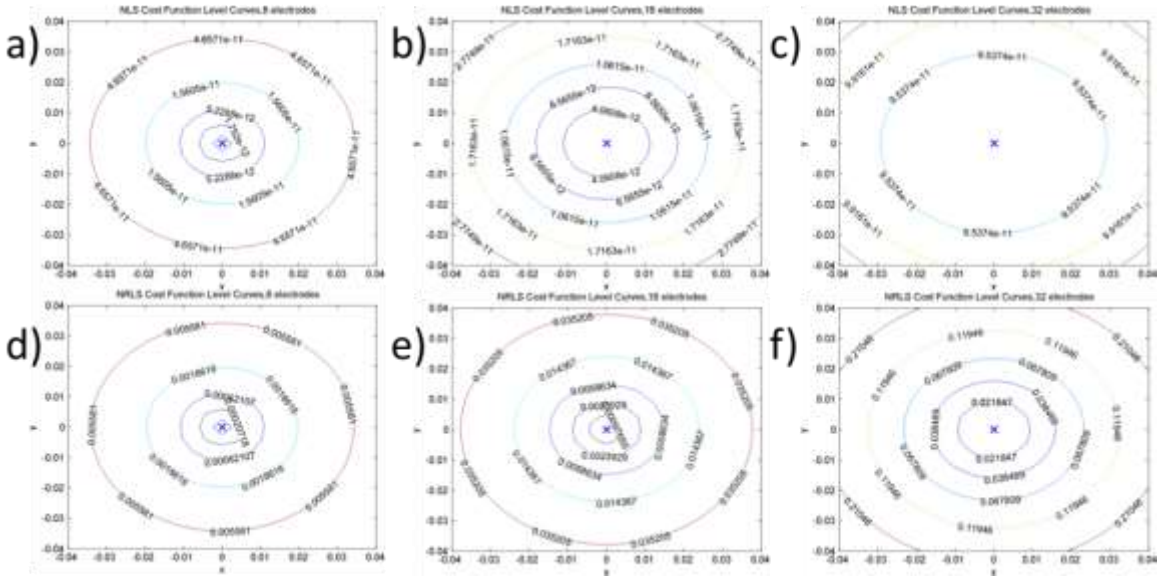

Figure 4. Cost level curves with 8, 16 and 32 electrodes for NLS and NRLS problems. Top row, NLS curves. Bottom row NRLS curves. a,d) 8 electrodes, b,e) 16 electrodes. c,f)32 electrodes

Simulations of 50 random positions using a fine mesh (6400 elements) were carried out. To avoid an inverse crime a coarse mesh of 576 elements was used for the optimization model. This coarse mesh model was used to highlight the dimensionality reduction that can be obtained. Problems were formulated using cost functions (5) and (6). Both were solved by the methods described in Table I. The initial point used for the optimal search was the origin. Simulations with different noise levels were carried: Noise free, SNR of 40 dB, 30.46 dB and 26.02 dB. Analysis of solutions of NLS and NRLS cost functions at are summarized in Table III and Table IV respectively. The tolerance used to residual changes was of 10^{-6} for all the methods. We limited the computational cost by setting a search time limitation of 25 seconds. The time limitation was checked between algorithms iterations, therefore the average search time was greater in most cases.

Table III. Solvers performance comparison for NLS with a 576 elements forward model at different SNR

Search Method	*Noise Free Data AST[s]*	*Noise Free Data MSE*	*AST[s] - SNR:40 dB*	*RMSE - SNR:40 dB*	*AST[s] - SNR:30.46 dB*	*RMSE - SNR:30.46 dB*	*AST[s] - SNR:26.02 dB*	*RMSE - SNR:26.02 dB*
LMDER	1.67E+01	1.66E-01	1.73E+01	1.66E-01	1.69E+01	1.66E-01	1.66E+01	1.65E-01
NLOPT	2.54E+01	1.65E-01	2.54E+01	1.67E-01	2.55E+01	1.66E-01	2.52E+01	1.67E-01
OPTI-FMINUNC	3.11E+01	3.81E-02	3.12E+01	2.87E-02	3.00E+01	9.77E-03	3.17E+01	1.23E-02
NOMAD	2.52E+01	1.88E-02	2.51E+01	**2.64E-04**	2.51E+01	2.68E-04	2.52E+01	1.70E-02
PSWARM	4.61E+01	3.91E-04	4.57E+01	1.93E-02	4.63E+01	4.98E-04	4.47E+01	7.36E-04
PATTERNSEARCH	2.64E+01	**2.70E-04**	2.62E+01	3.06E-04	2.64E+01	3.34E-04	2.63E+01	**6.73E-04**

FMINSEARCH	4.15E+01	1.03E-02	4.20E+01	1.04E-02	4.27E+01	**2.66E-04**	4.24E+01	1.13E-02
AST: Average Search Time(seconds) *MSE: Mean Squared Error*								

Table IV. Solvers performance comparison for NRLS with a 576 elements forward model at different SNR

Search Method	*Noise Free Data AST [s]*	*Noise Free Data MSE*	*AST[s] - SNR:40 dB*	*MSE - SNR:40 dB*	*AST[s] - SNR:30.46 dB*	*MSE - SNR:30.46 dB*	*AST[s] - SNR:26.02 dB*	*MSE - SNR:26.02 dB*
LMDER	2.13E+01	1.34E-01	2.11E+01	5.10E-02	2.15E+01	4.29E-02	2.16E+01	4.96E-02
NLOPT	2.54E+01	3.58E-02	2.53E+01	2.99E-02	2.53E+01	3.72E-02	2.54E+01	3.83E-02
OPTI-FMINUNC	3.13E+01	1.96E-02	3.14E+01	1.92E-02	3.13E+01	2.23E-02	3.16E+01	2.31E-02
NOMAD	2.50E+01	2.22E-02	2.50E+01	2.23E-02	2.50E+01	2.22E-02	2.50E+01	2.59E-02
PSWARM	4.77E+01	**3.88E-04**	4.60E+01	**3.52E-04**	4.65E+01	**3.15E-04**	4.75E+01	**4.03E-04**
PATTERNSEARCH	2.60E+01	2.24E-02	2.62E+01	2.24E-02	2.63E+01	2.24E-02	2.64E+01	2.28E-02
FMINSEARCH	4.60E+01	3.48E-02	4.61E+01	3.50E-02	4.61E+01	3.47E-02	4.66E+01	2.46E-02
AST: Average Search Time(seconds) *MSE: Mean Squared Error*								

Figure 5 shows the MSE distribution versus the real radius position of the object referenced at the tomograph center. It can be seen in the Figure 5 that LMDER and NLOPT were often not able to find the optimal solution. This was because methods found local optimal solutions close to the origin. Estimation with MSE less than $2.5 \cdot 10^{-3}$ for a radius position less than 0.7 was obtained by other methods. Estimation close to the boundary showed larger errors except for PATTERNSEARCH method that showed MSE less than $1.5 \cdot 10^{-3}$. This suggests the existence of local optimal close of the boundary or excessive time limitation for points far away of initial point.

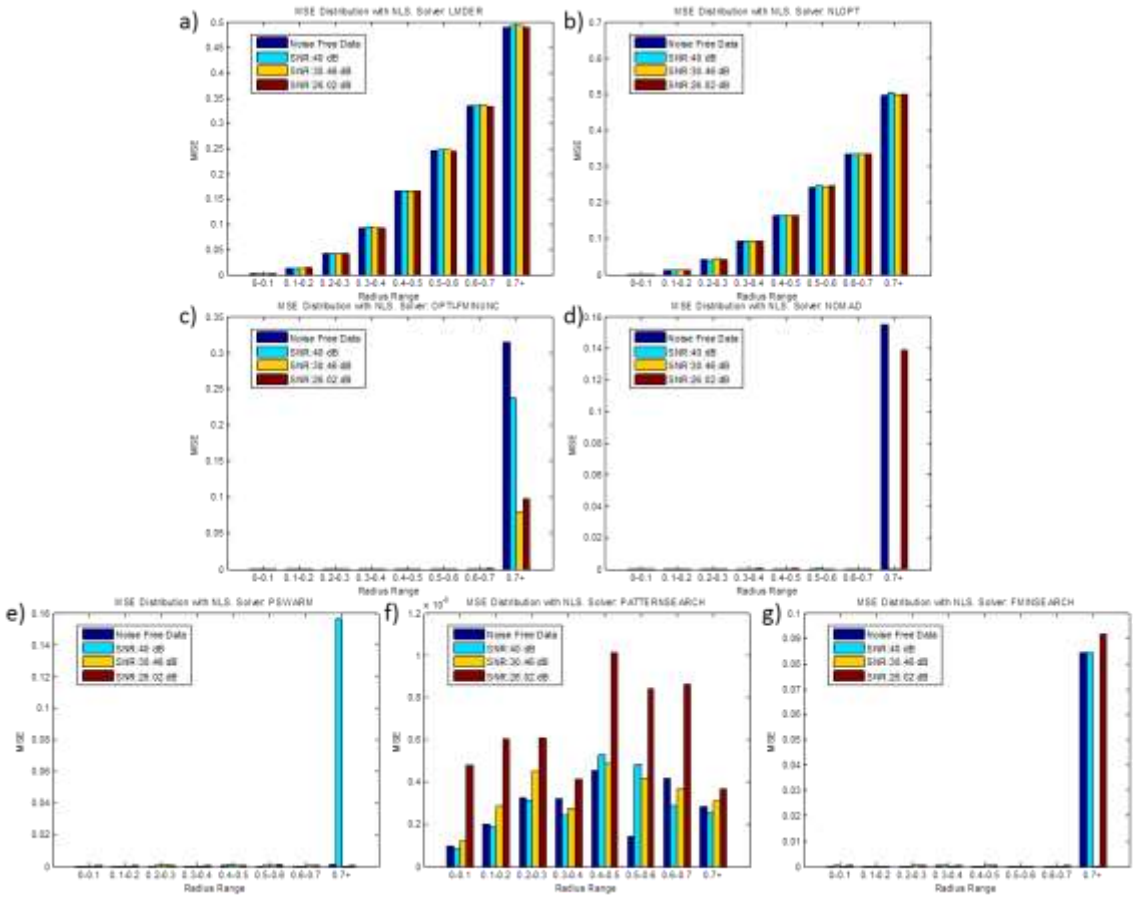

Figure 5. NLS solutions MSE vs. target radial distribution by several solvers. Note that figures have different scaling on vertical axis. a) LMDER b) NLOPT c) OPTI- FMINUNC d) NOMAD e) PSWARM f) PATTERNSEARCH g) FMINSEARCH

The NRLS solutions in Figure 6 show MSE less than $8 \cdot 10^{-2}$ estimation by all methods for radius less than 0.7. Largest MSE were found at positions close to boundary at radius greater than 0.7 with values over 0.15 for all solvers except PSWARM. This was the only method with MSE less than $1.5 \cdot 10^{-3}$ at all radius range for all the noise conditions.

No significant effects of the noise level were found for NLS and NRLS solutions. The best solutions were obtained in NLS except in the higher noise level case situation.

The overall best solvers results were gradient free optimization methods PATTERNSEARCH and PSWARM, however the last one required longer average search time.

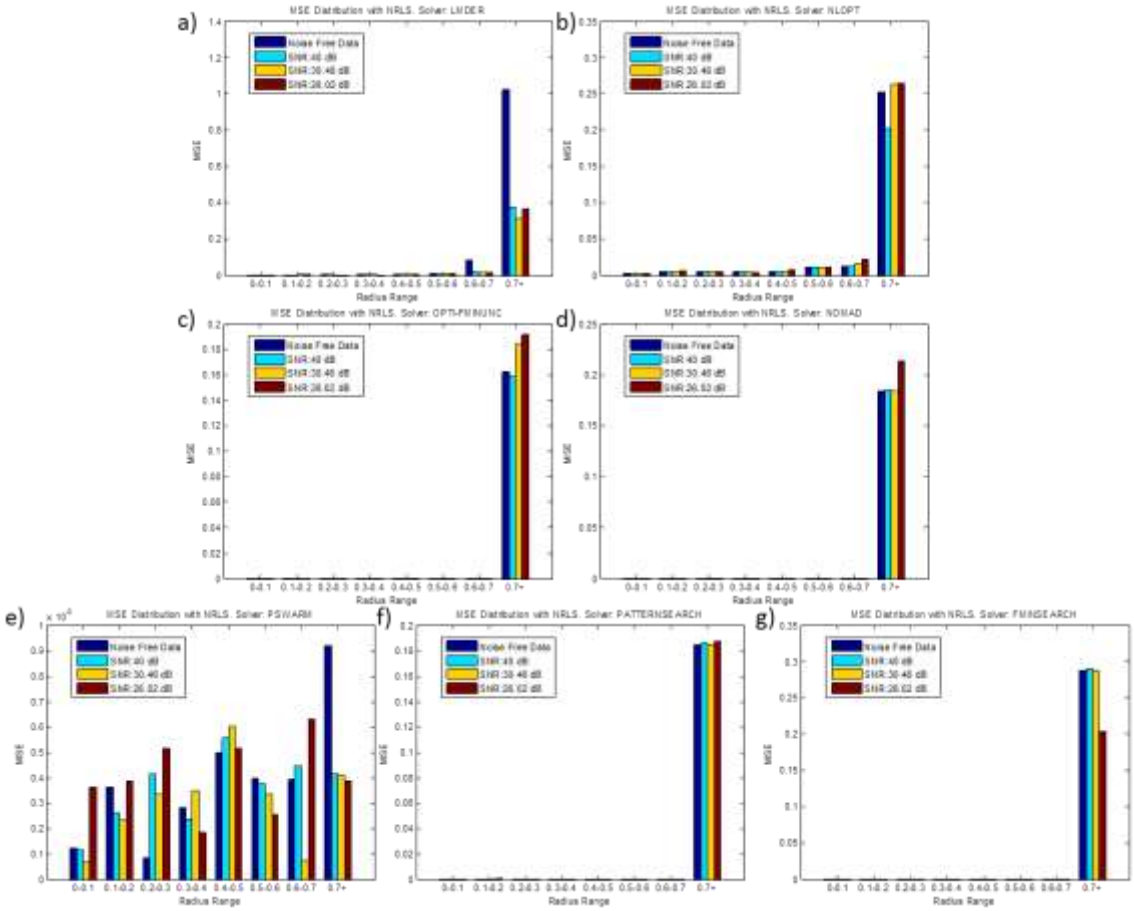

Figure 6. NRLS solutions MSE vs. target radial distribution by several solvers. Note that figures have different scaling on vertical axis. a) LMDER b) NLOPT c) OPTI- FMINUNC d) NOMAD e) PSWARM f) PATTERNSEARCH g) FMINSEARCH

4.1.2 Data Driven Models Approach

An evaluation of the effect of the estimation using 8, 16 and 32 electrodes was carried out. The simulations use the same mesh of 6400 elements. The same set of random points was used for model training in each case. Another set of random points was used for model testing. Results can be found on Table V. The results show improvement in the estimation accuracy by using more electrodes, this result contrasts with the one obtained for optimization methods. This might be due that data driven models weight the measurements, however optimization methods must deal with all the measurements.

Table V. Models Position MSE with tomograph of 8, 16 or 32 electrodes.

Model	*8 Electrodes*	*16 electrodes*	*32 Electrodes*
Polar Model	3.1380E-4	2.9088E-5	2.4964E-5
Cartesian Model	1.1327E-2	2.5803E-4	4.5674E-5

The models were calculated by using 1100 random training points obtained with the fine mesh model. The models were obtained and tested using free noise data and noises added with a SNR of 40 dB, 30.46 dB and 26.02 dB. The obtained models performance was tested using 400 random test positions. Results are summarized in Table VI.

Table VI. Position Estimation Error with Data Driven Models Approach

Model	*Average Calculation Time*	*Noise Free Data RMSE*	*RMSE - SNR:40 dB*	*RMSE - SNR:30.46 dB*	*RMSE - SNR:26.02 dB*
Polar Model	3.53E-08	2.55E-05	1.22E-04	4.48E-04	9.62E-04
Cartesian Model	6.41E-09	1.37E-04	2.47E-04	5.89E-04	1.13E-03

A 16 electrode system was used to evaluate the behaviour of methods in noisy situations. Calculation time is greater for the Polar than the Cartesian model because their outputs are needed for angle estimation. A MSE reduction was found by using the polar model approach (Table VI). However, it had increased MSE for objects positioned at the origin (Figure 7 a-d). In this case, the accuracy of the results of both models depends on the noise level, as SNR decreases (increased noise level) the position estimation MSE increases.

In Figure 7 the radial distribution of the position MSE is shown for the four simulated cases. It can be observed that the largest position error for the Cartesian model is close the boundary, while the Polar model has increased error at the center the tomograph. However, MSE less than $6.5 \cdot 10^{-3}$ were obtained in all the simulated situations.

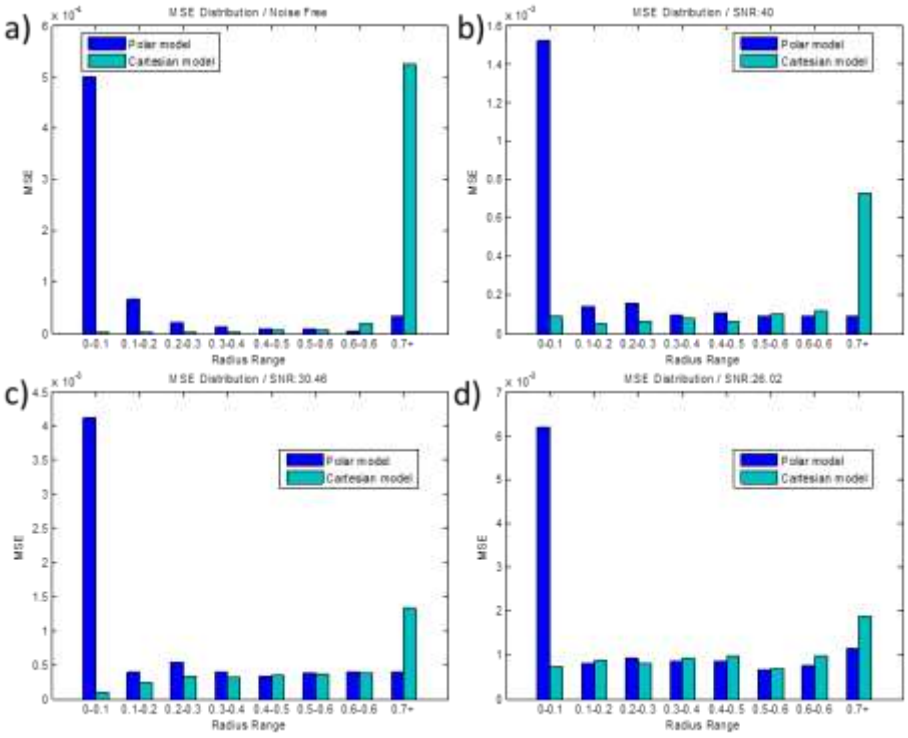

Figure 7. MSE distribution at several radius ranges with different SNR.

The MSE distribution shown by the Cartesian model was unexpected, because is well known that the sensitivity is higher close the boundary in EIT. We believe that this increase in the sensitivity at the boundary could be the reason of the error by making the linearization not valid in those zones. The increased error in the center in Polar model could be explained by an increased angle estimation error in that zone.

These results suggest that a combination of the two models can reduce the position estimation error by selecting one of two presented models output based object radius position. As this value is unknown we used the estimated radius $\hat{r}$ obtained by the Polar model. We set an estimated radius limit value r_l to output selection. We choose $r_l = 0.5$ based on results shown in Figure 7a-d.

$$\hat{X}_C = \begin{cases} \hat{X}\ (Cartesian\ model\ output) & \Theta_r\ U_e < r_l \\ \hat{X}_{\hat{r},\hat{\theta}}\ (Polar\ model\ output\ in\ cartesian\ coordinates) & \Theta_r\ U_e > r_l \end{cases} \quad (17)$$

4.1.3 Model robustness

This section illustrates the robustness of the model predictions when the conductivity of the medium changes and the model is not updated to take into account this new setting. Figure 8 shows incremental MSE due positive and negative changes in medium conductivity. Polar model is more sensitive, probably because its angular estimation depends of Cartesian model output. These results show the dependence of the results on the underlying assumptions used to build the model. If changes in the medium are important, then this variable should be included in the model and the training data set should take into account the more likely variations of this variable.

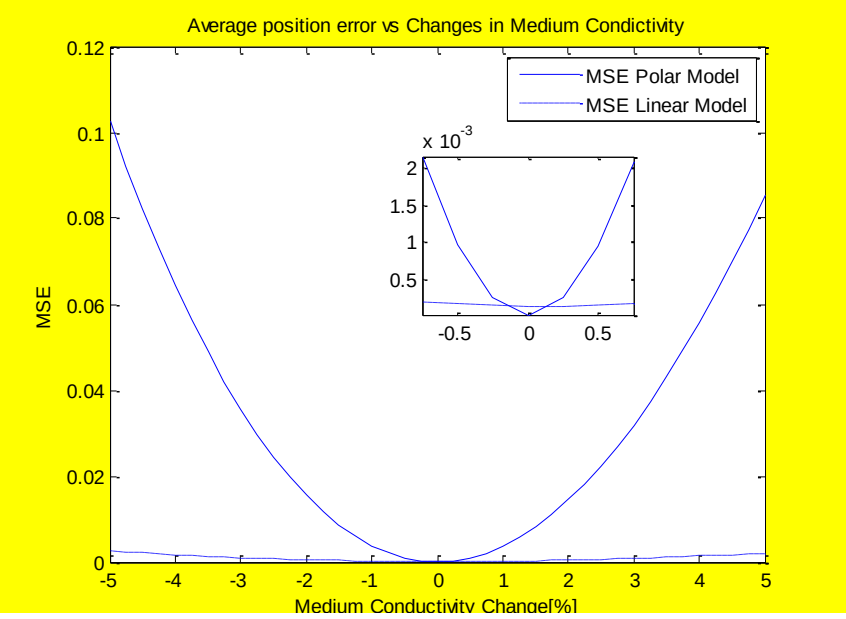

Figure 8. MSE obtained by changes in medium conductivity.

5 EXPERIMENTAL RESULTS

The hardware setup consists of a circular section vessel of 225-mm diameter filled with 130mm of tap water. The phantom had 16 equidistant stainless-steel electrodes of 30mm diameter on its boundary. A 40-mm diameter PVC pipe filled with sand was used as a target. Measured medium conductivity was $2.66 \cdot 10^{-4}[S/m]$. Target conductivity could not be measured but it was estimated by NLS at $5.9 \cdot 10^{-5}[S/m]$. Electrodes impedance was estimated by minimizing the squared norm of the difference between output simulation of homogeneous condition of calibrated model and measured voltages in the same condition. A current of 6.5 mA at 1 kHz with a neighborhood injection/measurement pattern was used. The object was manually displaced and had a pattern on its top. An USB camera captured the image of the object and the position was calculated by image processing. The process consisted in locating the object pattern to find its position relative to the phantom contour. The obtained object position was verified a posteriori by visual inspection of the images. A set of 1496 EIT contour voltages data and object positions were finally collected. The position measurements were referenced using the center of the vessel as origin.

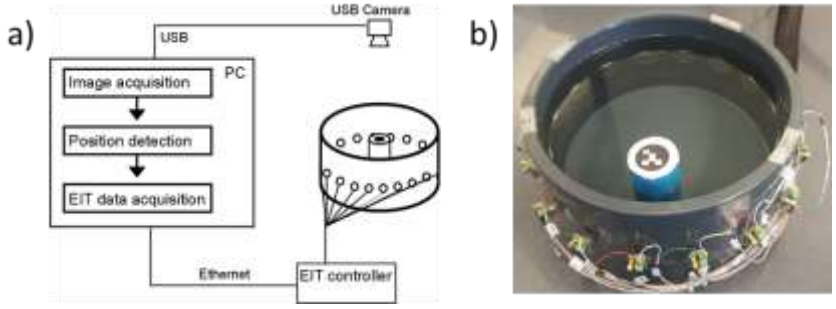

Figure 9. a) Experimental setting diagram. b) Hardware setup.

5.1 Experimental Results

5.1.1 Optimization approach

We obtained a total of 1496 data points. Each one is an object position obtained by image processing and a set of 208 contour voltages measurement. We reserved a set of 396 randomly selected data points for testing purposes. The other data points were used for model calibration in the optimization approach and the data driven models approach. The model was calibrated by using the method described in [47]. Optimization approach was formulated using cost functions (5) and (6) . Both were solved by PSWARM and PATTERN SEARCH methods because they showed less error in simulations. The search methods parameters used were the same that the ones used in simulations.

Table VII summarizes the results for both problems. Less MSE is obtained in the NRLS optimization problem. By comparing the solvers performance, PATTERNSEARCH method get less MSE and average search time.

Table VII. Experimental Position Estimation Error with Optimization approach.

Search Method	*NLS AST*	*NLS MSE*	*NRLS AST*	*NRLS MSE*

PSWARM	4.772E+01	2.077E-03	4.808E+01	1.034E-03
PATTERNSEARCH	2.630E+01	1.953E-03	2.632E+01	9.881E-04

In Figure 10 the MSE distribution of PSWARM and solutions according the real radius position is shown for NLS and NRLS problems. It can be seen that MSE smaller than 0.005 was obtained for both methods. Errors are increased at medium radius values, while the less MSE is found closer to the origin. Increased MSE close to boundary, as in simulations, were not found in experimental results. Furthermore, smaller MSE was found for PATTERNSEARCH compared with the simulation results, however the same relation was not obtained using PSWARM.

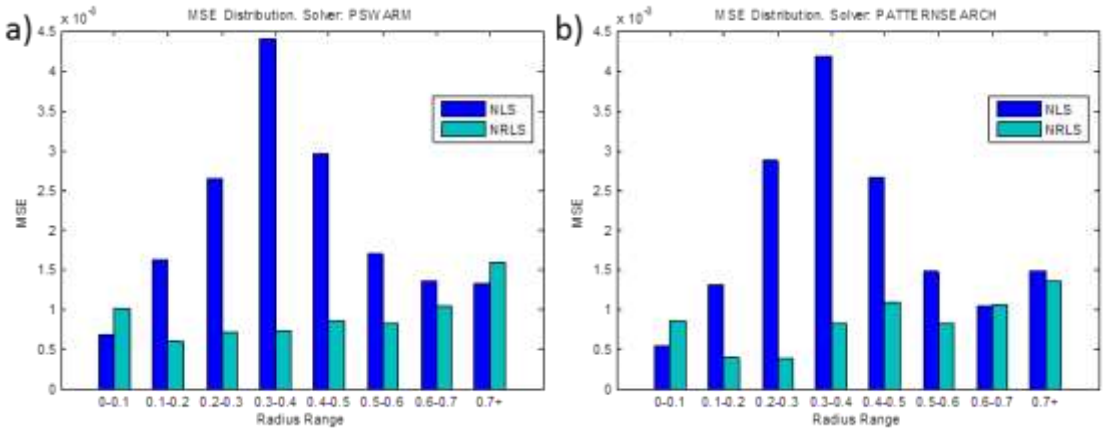

Figure 10. Experimental MSE Distribution for optimization approach. a) PSWARM solutions. b) PATTERNSEARCH solutions.

5.1.2 Data Driven Models Approach

The models were obtained using 1100 random training points. The same 396 testing position data used for optimization approach were used for evaluation also here. We included now the combined model proposed based on simulations results. The model output is the Cartesian model output for estimated radius less than 0.5 (according magnitude estimation of polar model), and in other case is the polar model output.

Table VIII. Experimental MSE and by Models Approach

Model	*Average Calculation Time*	*Estimated position MSE*
Polar Model	5.304E-05	4.00E-04
Cartesian Model	7.610E-06	4.63E-04
Combined Model	6.180E-05	3.98E-04

A resume of the three models performance is shown in Table VIII. The obtained MSE is similar to simulations results. It can be seen that the combined model achieved a slight MSE improvement over the other models. In Figure 11 the MSE distribution is shown. It can be seen a reduction on the error at radius close to zero and the boundary by the combined model. At range of radius 0.4-0.5

combined model shows an error greater than both models. This is an effect of the chosen parameter value $r_l = 0.5$ in the output selection criteria of the combined model.

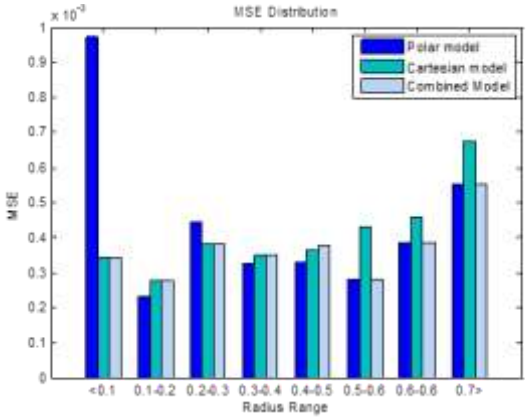

Figure 11. Experimental MSE Distribution for data driven models.

6 DISCUSSION

The results obtained for position estimation using simulations have illustrated that by incrementing the number of electrodes the data driven methods improve their accuracy. Optimization approaches, however seems not to be sensitive to this factor, since at the neighborhood of optimal point the NLS and NRLS cost functions becomes more flat. Several meshes with different number of elements were evaluated. It was found that coarse meshes had multiple local minimum close to the optimum. This was not found in finer meshes, however, it could be that local solutions becomes closer to the global solution.

Increasing noise level does not have a significant effect on the accuracy of the results obtained by optimization methods. Data driven models, instead, are more sensitive to his factor. An increase in the position estimation error is obtained as noise level increases. However, smaller MSE is obtained by data driven models than the one obtained by optimization methods for all noise levels and noise free simulation case.

Optimization approaches using gradient based algorithms had a poor performance. Almost all the solvers showed large MSE when the object position was close of the boundary. This suggests the existence of local minimum in cost surface when objects are close to boundary. The smaller MSE for the NLS problem was obtained by PATTERN-SEARCH algorithm. The use of NRLS problem improved the solutions for almost all search methods. Larger errors still exist close to the boundary positions. However, PSWARM solutions had a MSE smaller than $1.5 \cdot 10^{-3}$ in all radius range and all noise situations. This difference in problems that share the same ideal optimal point is explained because the NRLS problem amplifies the small errors in measurements providing a more sensitive cost function in this situation.

Data driven models simulation results shows that MSE of Polar coordinates model is smaller than the Cartesian coordinates model close to the boundary, but it is worst at the central position. However, MSE less than $6.5 \cdot 10^{-3}$ were obtained by all the simulated situations. Based in these

results a third approach base on the combination of both models was proposed. Simulations were carried to show the robustness of the estimations against changes in medium conductivity. Both models increase PE errors, however Cartesian model is more robust. Polar model has smaller error only under the nominal medium conductivity.

The experimental results confirm the simulation results. Position estimation with a MSE smaller than $4.5 \cdot 10^{-3}$ was obtained by PSWARM and PATTERN-SEARCH methods for both cost functions. The last algorithm obtained the smallest average search time and MSE. Solutions of NLS had smaller MSE than NRLS only for radius values under 0.1. Furthermore, the optimization approach showed good experimental position estimation with MSE smaller than $4.5 \cdot 10^{-3}$. The main advantage of this method is that it requires only a few experimental data points to achieve a model calibration.

Data driven modelling results have associated an MSE smaller than $1 \cdot 10^{-3}$ for all data driven models. The error distribution was similar to simulations but smaller error was found at extreme radius. The combined model decreases the MSE in 14% compared with the Cartesian model approach.

Data driven approaches showed smaller errors and more than $7 \cdot 10^{5}$ times faster estimation than the optimization approach. Mean squared errors smaller than $1 \cdot 10^{-3}$ were obtained in experimental results.

7 CONCLUSION

The estimation of low dimensional features can be carried out by optimization and data driven approaches. Optimization approaches estimate the low dimensional features by minimizing a cost function considering the difference between the boundary voltage measurements and the ones provided by the complete electrode model. Data driven models provide estimations given by a direct mapping between the low dimensional feature and the voltage measurements. Both methods are sensitive to experimental conditions such as number of electrodes and signal-noise ratio. Optimization methods are also sensitive to modelling errors. The use of weighted cost functions and derivative free optimization algorithms can reduce the effect of modelling errors. Data driven approaches instead parameterize the relationship between the low dimensional feature and boundary voltages. These methods do not require the use of an explicit model for the EIT sensor and objects. However, the estimation of the parameters requires a large data set.

Results obtained from the estimation of an object position show that for this application the optimization based approaches were very sensitive to model discretization. The use of NRLS and derivate free optimizations algorithms provided better estimates compared to the use of RLS and gradient based algorithms. Data driven approaches are simpler, computationally less expensive and accurate than optimization approach, however their used is limited by the existence of an appropriate relationship between features and output voltages. In addition, they require a large data training set to take into account all the possible operational conditions. The validity of the model will depend on the training data set and on the parametrization. Furthermore, optimization approaches are computationally more expensive, but they require fewer data points to calibrate the

FEM model. Further work will analyse the use of data driven approaches trained by data obtained from calibrated FEM models. This will enable to train data driven models using less experimental data. In addition, the estimation of multiple features using statistical methods is also part of our current research interest.

8 ACKNOWLEDGMENTS

Support from CONICYT-PCHA/National PhD/2015-21150185 is acknowledged by S. Vergara.

BIBLIOGRAPHY

1. Dyakowski T, Jeanmeure LFC, Jaworski AJ. Applications of electrical tomography for gas–solids and liquid–solids flows — a review. Powder Technol. 2000 Oct 31;112(3):174–92.

2. K. Primrose, C. Qiu. Electrical impedance tomographic sensor systems. Sens Rev. 2000 Sep 1;20(3):189–95.

3. Holder D, Institute of Physics (Great Britain), editors. Electrical impedance tomography: methods, history, and applications. Bristol ; Philadelphia: Institute of Physics Pub; 2005. 456 p. (Series in medical physics and biomedical engineering).

4. Wang M. Industrial tomography: systems and applications. Elsevier; 2015.

5. Brown BH. Medical impedance tomography and process impedance tomography: a brief review. Meas Sci Technol. 2001;12(8):991.

6. Harikumar R, Prabu R, Raghavan S. Electrical Impedance Tomography (EIT) and Its Medical Applications: A Review. Int J Soft Comput Eng. 2013;3(4):2231–2307.

7. Bera TK. Bioelectrical Impedance Methods for Noninvasive Health Monitoring: A Review. J Med Eng. 2014 Jun 17;2014:e381251.

8. Minhas AS, Reddy MR. Neural network based approach for anomaly detection in the lungs region by electrical impedance tomography. Physiol Meas. 2005 Aug 1;26(4):489–502.

9. Ohin Kwon, Jeong Rock Yoon, Jin Keun Seo, Eung Je Woo, Young Gu Cho. Estimation of anomaly location and size using electrical impedance tomography. IEEE Trans Biomed Eng. 2003 Jan;50(1):89–96.

10. Ceccio SL, George DL. A Review of Electrical Impedance Techniques for the Measurement of Multiphase Flows. J Fluids Eng. 1996;118(2):391.

11. Warsito W, Fan L-S. ECT imaging of three-phase fluidized bed based on three-phase capacitance model. Chem Eng Sci. 2003 Feb;58(3–6):823–32.

12. Lampinen J, Vehtari A, Leinonen K. Application of Bayesian neural network in electrical impedance tomography. In: Neural Networks, 1999 IJCNN'99 International Joint Conference on. IEEE; 1999. p. 3942–7.

13. Vauhkonen M, Vadasz D, Karjalainen PA, Somersalo E, Kaipio JP. Tikhonov regularization and prior information in electrical impedance tomography. IEEE Trans Med Imaging. 1998;17(2):285–293.

14. Vauhkonen M. Electrical impedance tomography and prior information. [Kuopio]: University of Kuopio; 1997.

15. Wang M. Inverse solutions for electrical impedance tomography based on conjugate gradients methods. Meas Sci Technol. 2001;13(1):101.

16. Kim MC, Kim S, Lee KJ, Kim KY. Improvement of the electrical impedance tomographic image for the two-phase system with adaptive element grouping technique. Meas Sci Technol. 2004 Jul 1;15(7):1391–401.

17. Rezajoo S, Hossein-Zadeh G-A. Reconstruction convergence and speed enhancement in electrical impedance tomography for domains with known internal boundaries. Physiol Meas. 2010 Nov 1;31(11):1499–516.

18. Kim BS, Khambampati AK, Kim S, Kim KY. Image reconstruction with an adaptive threshold technique in electrical resistance tomography. Meas Sci Technol. 2011 Oct 1;22(10):104009.

19. Yasin M, Böhm S, Gaggero PO, Adler A. Evaluation of EIT system performance. Physiol Meas. 2011 Jul 1;32(7):851–65.

20. De Munck JC, Faes TJC, Hermans AJ, Heethaar RM. A Parametric Method to Resolve the Ill-Posed Nature of the EIT Reconstruction Problem: A Simulation Study. Ann N Y Acad Sci. 1999 Apr;873(1 ELECTRICAL BI):440–53.

21. Watzenig D, Brandner M, Steiner G. A particle filter approach for tomographic imaging based on different state-space representations. Meas Sci Technol. 2007 Jan 1;18(1):30–40.

22. Khambampati AK, Ijaz UZ, Lee JS, Kim S, Kim KY. Phase boundary estimation in electrical impedance tomography using the Hooke and Jeeves pattern search method. Meas Sci Technol. 2010 Mar 1;21(3):035501.

23. Wei K (Hsin-Y, Qiu C-H, Primrose K. Super-sensing technology: industrial applications and future challenges of electrical tomography. Philos Trans R Soc Math Phys Eng Sci. 2016 Jun 28;374(2070):20150328.

24. George DL, Torczynski JR, Shollenberger KA, O'Hern TJ, Ceccio SL. Validation of electrical-impedance tomography for measurements of material distribution in two-phase flows. Int J Multiph Flow. 2000 Apr;26(4):549–81.

25. J. R. Torczynski, T. J. O'Hern, D. R. Adkins, N. B. Jackson, K. A. Shollenberger. Advanced Tomographic Flow Diagnostics for Opaque Multiphase Fluids. Sandia National Laboratories, Albuquerque, NM.; 1997. Report No.: SAND97-1176.

26. S. Vergara, D. Sbarbaro. Position estimation based on Electrical Impedance Tomography. In: 8th World Congress on Industrial Process Tomography. Iguassu Falls, Brazil; 2016.

27. Jin J-M. The finite element method in electromagnetics. Third edition. Hoboken. New Jersey: John Wiley & Sons Inc; 2014. 846 p.

28. Johansen TA. Identification of non-linear systems using empirical data and prior knowledge—an optimization approach. Automatica. 1996 Mar;32(3):337–56.

29. Sjöberg J, Zhang Q, Ljung L, Benveniste A, Delyon B, Glorennec P-Y, et al. Nonlinear black-box modeling in system identification: a unified overview. Automatica. 1995 Dec;31(12):1691–724.

30. Schölkopf B, Smola AJ. Learning with Kernels: Support Vector Machines, Regularization, Optimization, and Beyond. MIT Press; 2002. 658 p.

31. Hastie T, Tibshirani R, Friedman J. The Elements of Statistical Learning [Internet]. New York, NY: Springer New York; 2009 [cited 2017 May 15]. (Springer Series in Statistics). Available from: http://link.springer.com/10.1007/978-0-387-84858-7

32. Cheney M, Isaacson D. Distinguishability in impedance imaging. Biomed Eng IEEE Trans On. 1992;39(8):852–860.

33. Koksal A, Eyuboglu BM. Determination of optimum injected current patterns in electrical impedance tomography. Physiol Meas. 1995;16(3A):A99.

34. Eyuboglu BM, Pilkington TC. Comments on distinguishability in electrical impedance imaging. IEEE Trans Biomed Eng. 1993;40(12):1328–1330.

35. Tang M, Wang W, Wheeler J, McCormick M, Dong X. The number of electrodes and basis functions in EIT image reconstruction. Physiol Meas. 2002;23(1):129.

36. Schullcke B, Krueger-Ziolek S, Gong B, Moeller K. Effect of the number of electrodes on the reconstructed lung shape in electrical impedance tomography. Curr Dir Biomed Eng [Internet]. 2016 Jan 1 [cited 2017 Mar 31];2(1). Available from: http://www.degruyter.com/view/j/cdbme.2016.2.issue-1/cdbme-2016-0110/cdbme-2016-0110.xml

37. Silvester PP, Ferrari RL. Finite Elements for Electrical Engineers. Cambridge University Press; 1996. 520 p.

38. Nissinen A, Kolehmainen VP, Kaipio JP. Compensation of Modelling Errors Due to Unknown Domain Boundary in Electrical Impedance Tomography. IEEE Trans Med Imaging. 2011 Feb;30(2):231–42.

39. Nissinen A, Kolehmainen V, Kaipio JP. Reconstruction of domain boundary and conductivity in electrical impedance tomography using the approximation error approach. Int J Uncertain Quantif [Internet]. 2011 [cited 2016 Aug 14];1(3). Available from: http://www.dl.begellhouse.com/journals/ijuq/vol1/i3/p203-222/

40. Nissinen A, Kolehmainen V, Kaipio JP. Compensation of errors due to incorrect model geometry in electrical impedance tomography. J Phys Conf Ser. 2010 Apr 1;224:012050.

41. Grychtol B, Lionheart WRB, Bodenstein M, Wolf GK, Adler A. Impact of Model Shape Mismatch on Reconstruction Quality in Electrical Impedance Tomography. IEEE Trans Med Imaging. 2012 Sep;31(9):1754–60.

42. A. Nissinen, L. M. Heikkinen, J. P. Kaipio. Approximation Errors in Electrical Impedance Tomography – An Experimental Study. In Bergen, Norway; 2007. p. 858–64.

43. Kaipio J, Somersalo E. Statistical and computational inverse problems. New York: Springer; 2005. 339 p. (Applied mathematical sciences).

44. Adler A, Lionheart WRB. Minimizing EIT image artefacts from mesh variability in finite element models. Physiol Meas. 2011 Jul 1;32(7):823–34.

45. Boyle A, Adler A. The impact of electrode area, contact impedance and boundary shape on EIT images. Physiol Meas. 2011 Jul 1;32(7):745–54.

46. Nissinen A, Heikkinen LM, Kaipio JP. The Bayesian approximation error approach for electrical impedance tomography—experimental results. Meas Sci Technol. 2008 Jan 1;19(1):015501.

47. Soni NK, Dehghani H, Hartov A, Paulsen KD. A novel data calibration scheme for electrical impedance tomography. Physiol Meas. 2003;24(2):421.

48. Currie J, Wilson DI. OPTI: lowering the barrier between open source optimizers and the industrial MATLAB user. Found Comput-Aided Process Oper. 2012;8–11.

49. Birgin EG, Martínez JM. Improving ultimate convergence of an augmented Lagrangian method. Optim Methods Softw. 2008 Apr;23(2):177–95.

50. Conn AR, Gould NI, Toint P. A globally convergent augmented Lagrangian algorithm for optimization with general constraints and simple bounds. SIAM J Numer Anal. 1991;28(2):545–572.

51. Rao SS, Rao SS. Engineering Optimization: Theory and Practice. John Wiley & Sons; 2009. 835 p.

52. Vaz AIF, Vicente LN. A particle swarm pattern search method for bound constrained global optimization. J Glob Optim. 2007 Sep 4;39(2):197–219.

53. Audet C, Dennis Jr JE. Analysis of generalized pattern searches. SIAM J Optim. 2002;13(3):889–903.

54. Adler A, Lionheart WRB. Uses and abuses of EIDORS: an extensible software base for EIT. Physiol Meas. 2006 May 1;27(5):S25–42.